# The assembly of microbial communities on red sandstone surfaces was shaped by dispersal limitation and heterogeneous selection

Bowen Wang [a, b], Chengshuai Zhu [a], Xin Wang [c], Tianyu Yang [d], Bingjian Zhang [a, c] and Yulan Hu [a*]

[a] Department of Archaeology, Cultural Heritage and Museology, Zhejiang University, Hangzhou, 310028, China.
[b] Department of Biology, Johns Hopkins University, Baltimore, MD, 21218, USA.
[c] Department of Chemistry, Zhejiang University, Hangzhou, 310028, China.
[d] Leshan Giant Buddha Grottoes Research Institute, Leshan Giant Buddha Scenic Area Management Committee, Leshan, 614000, China.

[*]Corresponding: hu_yulan@zju.edu.cn

## Abstract

Understanding the role of microbiota on stone surface is essential for developing effective grottoes conservation strategies. However, ecological feature of microbial communities on stone surface have been rarely investigated systematically. In this study, we explored diversity, assembly, and functional profiles of microbial communities on the red sandstone surface of the Leshan Giant Buddha from microbial ecology perspective. The results show that Proteobacteria, Actinobacteria, Cyanobacteria, and Ascomycota are the dominant phyla. Fundamental metabolic pathways are maintained during the formation of visually distinguishable microbial communities, but gene profiles vary across microbial communities of different colors. Ecological modelling suggests that selective pressure from the harsh stone surface environment fostered the interplay of dispersal limitation and heterogeneous selection during community assembly. The assembly of visually distinct microbial communities is linked to a narrower ecological niche, higher proportion of habitat specialists, and sparser network structure. Microbial-mediated ammonium assimilation and nitrogen mineralization might be the two prominent processes that contribute to stone biodeterioration. This study deepens our understanding of the assembly mechanisms and functional potentials of microbial communities on stone cultural heritage surfaces, provides microbial ecological insights for the conservation of these cultural treasures.

**Importance:** Minimal systematically research on the ecological interpretation of stone biodeterioration. This study reports dispersal limitation and heterogeneous selection shape the microbial community assembly responsible for the biodeterioration of red sandstone. Furthermore, fundamental metabolic processes of microbial communities, such as ammonium assimilation and nitrogen mineralization, are identified as contributors to stone biodeterioration. This study improves our understanding of microbial community assembly and their functional roles, providing a microbial ecological basis for developing effective strategies for the conservation of stone cultural heritage.

**Keywords:** Community assembly; Microbial community; Microbial diversity; Microbial ecology; Stone; Cultural Heritage

## 1. Introduction

Grottoes are a common form of stone cultural heritage. The stone surface of grottoes are integral components of ecosystems, providing critical habitats for microbial communities, serving as crucial habitats for microorganisms organized into diverse microbial communities[1-3]. Under specific conditions, these microbial communities can reinforce the stone through metabolic processes like biomineralization[1,4-7]. However, in most cases, the microbial communities on stone surface not only diminish the aesthetic value of the artifacts by obscuring and deteriorating the carvings but may also, in some cases, compromise the structural integrity of the grottoes through severe erosion processes[3,8-11]. Therefore, cleaning and controlling the formation of microbial communities on stone surface are essential tasks in the conservation of stone cultural heritage. Understanding the characteristics of microbial communities on stone surface is crucial for developing effective strategies to mitigate microbial deterioration. Currently, research in this field primarily focuses on the taxonomic diversity of microorganisms and their biogeochemical cycling and metabolic capabilities. These studies have revealed the key microbial groups involved in the biodeterioration of stone cultural heritage and their associated biogeochemical processes and metabolic responses[10,12-17]. However, ecological understanding of how microbial communities assemble on the stone surface remains significantly limited.

The ecological mechanisms that govern microbial community assembly are one of the main scientific questions in ecological research[18-20]. It is generally believed that the assembly of local microbial communities is controlled by the combined effects of deterministic and stochastic processes[21-23]. Deterministic processes are used to describe the traditional niche-based theory, which hypothesize that species traits, interspecific interactions, and environmental factors govern community structure[24,25]. In contrast, stochastic processes are based on the neutral theory, which illustrate that community assembly is driven by stochastic events such as birth, death, colonization, extinction, and speciation[26,27]. Another quantitative framework for understanding ecological interactions and community assembly is the dissimilarity-overlap curve (DOC), which describes how community dissimilarity changes with the overlap of shared taxa[28]. The niche on the stone surface exposes microorganisms to environmental stresses (abiotic and biotic constraints that limit species productivity and ecosystem development[29]) from nutrient and water scarcity, as well as extreme fluctuations in temperature, humidity, and solar UV radiation[1]. Generally, environmental stress increases deterministic assembly while reducing stochastic assembly, because species with higher tolerance or adaptability to these stressors tend to survive and thrive[29-31]. Furthermore, under high-stress conditions, microbial dispersal limitations are enhanced because elevated stress impedes colonization and successful establishment[29,32,33]. A recent study on microbial communities on limestone surface revealed that bacteria and fungi in this environment are primarily dominated by the mutual effect of dispersal limitation (stochastic processes) and homogeneous selection (deterministic processes)[3]. However, it is currently unknown whether such community assembly mechanisms are specific to certain stone type, geographic location, or influenced by other factors.

The Leshan Giant Buddha, a world-renowned UNESCO World Heritage site, is a typical example of red sandstone grotto cultural heritage. Previous studies found abundant nitrogen-metabolizing microorganisms and ammonia monooxygenase genes, linked to biodeterioration, on the surface of the Leshan Giant Buddha, which suggests that the deterioration of the stone is closely related to microbial growth[34-36]. The cleaning of stone surface is a crucial task for conservation of the grotto. The current issue is that despite regular cleaning of the stone surface by heritage conservators, visually distinguishable microbial communities persistently reappear after each cleaning. However, our understanding of how microorganisms assemble microbial communities on the stone surface of the Leshan Giant Buddha, as well as on other red sandstone surfaces, remains limited. There is an essential need to investigate the mechanisms by which microbes survive and how they form microbial communities within such ecosystems under various environmental stresses from the perspective of microbial ecology. Therefore, this study uses the Leshan Giant Buddha, a UNESCO World Heritage site, as a case study to provide a comprehensively microbial ecological evaluation to the microbial communities on the surface of this red sandstone cultural heritage. The goal of this study is to examine whether the ecological characteristics of microbial communities on red sandstone surfaces are associated with adaptation to harsh environmental conditions. Specifically, we investigate how these microorganisms assemble into stable communities under repeated wet-dry cycles, nutrient limitations, and UV radiation, and what functional capacities they exhibit. Additionally, in this study, we also performed network and niche metrics analysis to better understand the assembly of microbial communities on the red sandstone surface. Network analysis reveals co-occurrence patterns and potential interactions among microbial taxa, while niche metrics such as niche breadth and overlap characterize habitat specialization and resource utilization. These niche-based analyses further allow us to distinguish between generalist (thrive across a wide range of conditions) and specialist (restricted to narrower ecological niches). Our focus extends beyond the interactions within the microbiota to include the interactions among microorganisms, environmental factors, and the stone substrate.

## 2. Results

### 2.1. Taxonomic composition varies by the color of microbial communities

Samples of three different types of visually distinguishable microbial communities, along with blank samples, were collected from the stone surface of the Leshan Giant Buddha. In general, the total 27 samples were grouped and named according to their respective colors (Bla, black; Gre, green; Whi, white; and CK, blank control) (Fig. 1). We then performed amplicon sequencing of conserved phylogenetic marker genes (16S and ITS rRNA) to identify bacteria and fungi within the microbial communities. After quality filtering and rarefaction, a total of 8,791 and 2,404 non-zero ASVs were obtained from the 16S and ITS sequences, respectively. Each group of data overlap with others, but they are not entirely identical or inclusive of each other (Fig. S1).

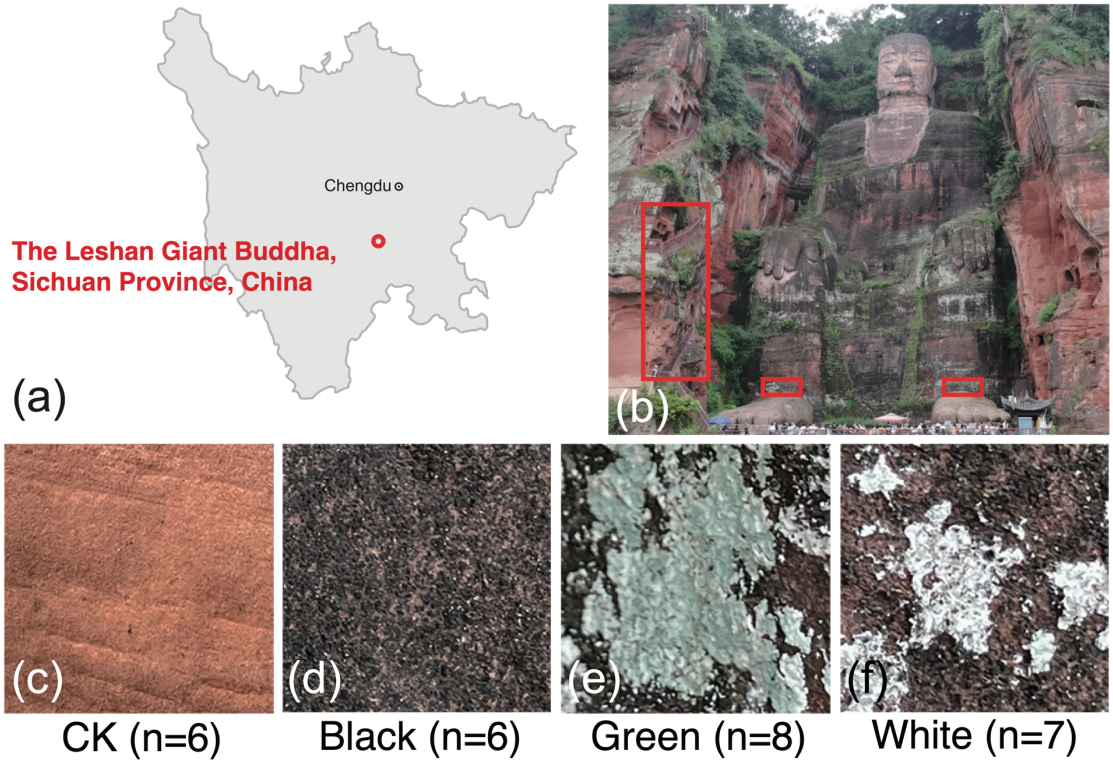


**Figure 1.** Representative examples and sampling of microbial communities on the red sandstone surface of the Leshan Giant Buddha. (a). Location of the Leshan Giant Buddha. (b). Sampling regions of the samples. Red boxes here indicate the specific sampling regions. (c). Representative examples of CK samples. (d). Representative examples of Black samples. (e). Representative examples of Green samples. (f). Representative examples of White samples. Notes: "n" in picture c-f represents the number of samples used in this study within each group.

To get taxonomic insights into the microbiota, we annotated the sequencing data, then visualized top 10 dominant phyla, top 20 dominant genus of bacteria (Fig. 2 a; Fig. S2 a; Table S1, S2) and fungi (Fig. 2 b; Fig. S2 b; Table S3, S4) across all samples. The results show that among all samples, Proteobacteria, Actinobacteria, and Cyanobacteria are the dominant top three phyla in bacteria, comprising at least 70% of the total bacteria in each sample. Ascomycota is the most dominant phylum in fungi, comprising at least 50% of the total fungi in each sample.

To estimate the separation pattern between each group of microbial communities, non-metric multidimensional scaling (NMDS) based on Bray-Curtis dissimilarity at the ASV level was performed and then conducted Anosim (analysis of similarities) and PERMANOVA (*i.e.*, adonis) tests (Fig. 2 e, f). The results show that both bacteria and fungi among the four groups of samples reveal significant and major differences ($P < 0.001$). In summary, the structure of microbial communities varies according to the coloration of the samples, which indicates distinct microbial compositions among samples of different colors.

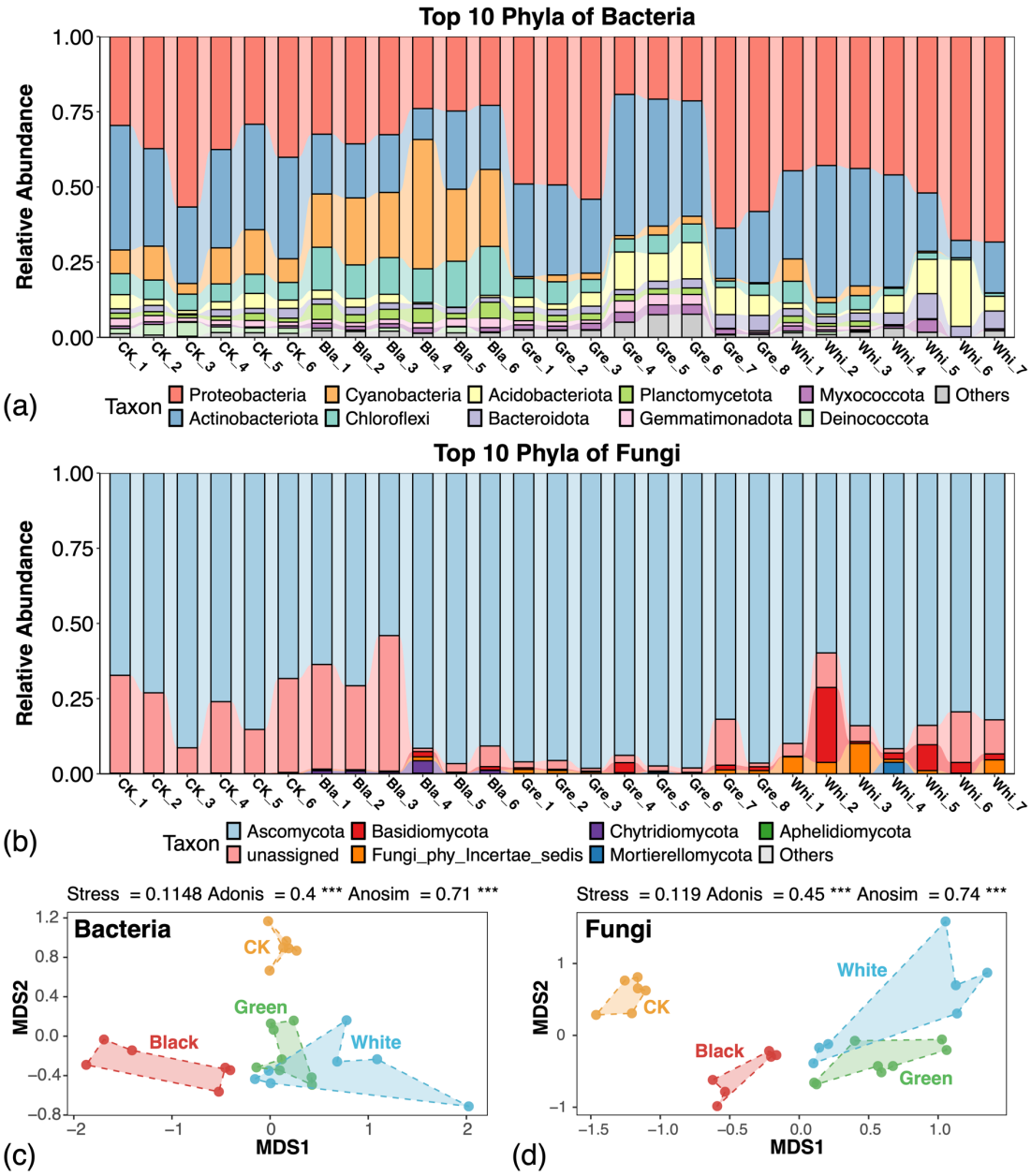


**Figure 2.** Taxonomic composition and distinct taxonomic structures of the microbial communities. (a). Relative abundances of dominant bacteria among all samples in phylum level. (b). Relative abundances of dominant fungi among all samples in genus level. (c). Non-metric multidimensional scaling (NMDS) ordination based on Bray-Curtis dissimilarities at the ASV level for bacteria. (d). Non-metric multidimensional scaling ordination based on Bray-Curtis dissimilarities at the ASV level for fungi. Notes: The triple asterisks *** represents the $P < 0.001$.

### 2.2. Dispersal limitation and heterogeneous selection dominants the assembly of red sandstone surface microbial communities

To characterize the assembly mechanism of the red sandstone surface microbial communities, we applied null model analysis[37,38] and DOC model analysis (Fig. 3)[28]. Null model analysis showed that both deterministic and stochastic processes controlled the assembly of microbial communities, but the relative importance of the two processes in community assembly vary

among sample types (Fig. 3 a, b). In general, dispersal limitation dominated the assembly of both bacteria communities (60.11%) and fungi communities (55.56%) on stone surface. Bacteria revealed overall elevated deterministic processes than fungi. Heterogeneous selection and dispersal limitation can explain about 91% of the assembly mechanism of the bacteria communities. While heterogeneous selection and dispersal limitation were also main processes for the assembly of fungi communities; drift played a more pivotal role in the assembly processes of fungi communities (20.23%) than in the bacteria ones (5.41%). Bacteria samples revealed significantly higher value of betaNTI than fungi ones (Fig. 3 c). Significant elevation of betaNTI was detected among White groups of bacteria samples comparing with CK (Fig. 3 d). By contrast, significant elevation of betaNTI was detected among Black as well as Green groups of fungi samples comparing with CK (Fig. 3 e). The DOC model analysis demonstrated a significantly negative correlation between overlap and dissimilarity in both bacteria and fungi communities ($P < 0.001$), which indicated a general dynamic and interspecific interaction within these microbial communities (Fig. 3 f, g). The fitted slope (Fns) was slightly higher in bacteria (0.3351) than in fungi (0.2691), which suggests that bacterial communities exhibited more rapid compositional turnover. These complex dynamic interactions among microorganisms in the microbiota might lead to competition within the shared niche for survival.

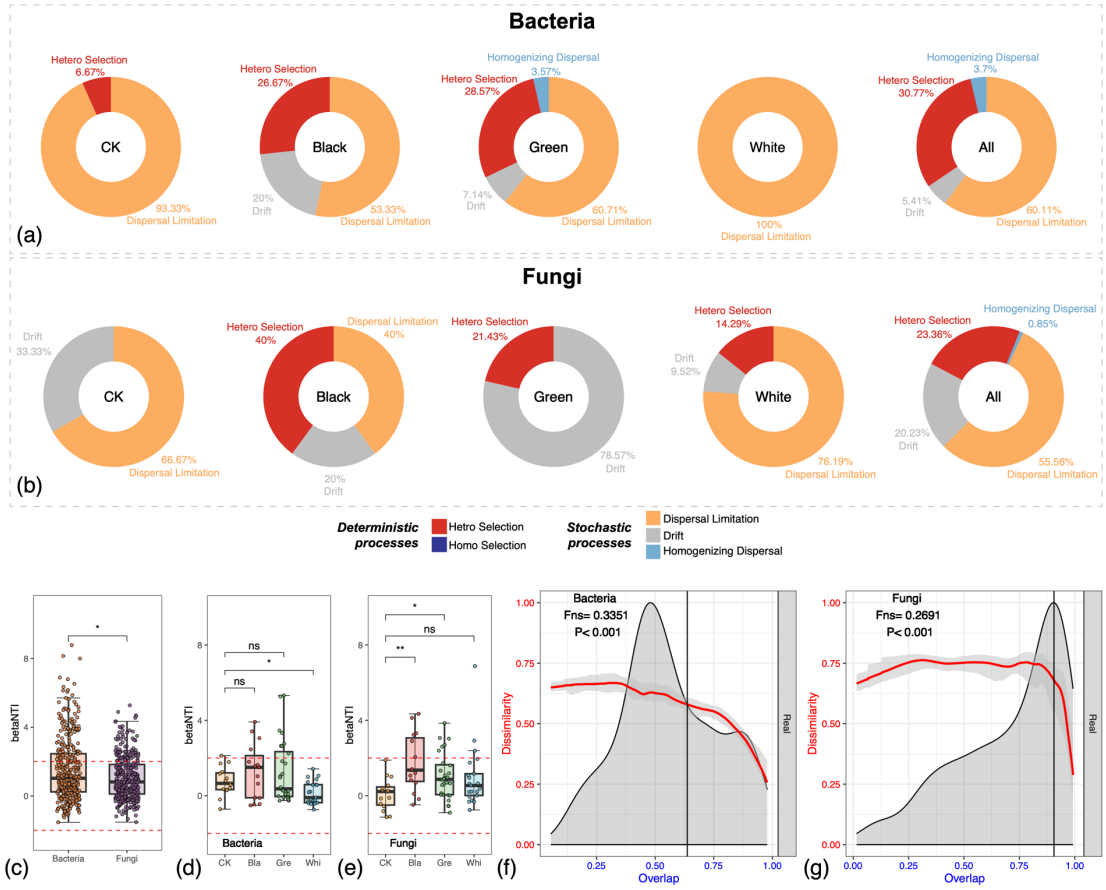


**Figure 3.** Assembly dynamics of the red sandstone surface microbial communities. (a). The relative importance of assembly processes in bacteria communities. (b). The relative importance of assembly processes in fungi communities. (c). The differences of betaNTI between bacteria and fungi communities. (d). Changes of betaNTI among three groups of bacteria samples comparing with CK. (e). Changes of betaNTI among three groups of fungi samples comparing with CK. (f).

Dissimilarity-overlap curve (DOC) analysis of the universality of bacteria dynamics among samples. (g). DOC analysis of the universality of fungi dynamics among samples.

**2.3. Specialization prevails over flexibility in microbial community formation on red sandstone surface**

To delve deeper into the dynamic interactions among microorganisms within the microbiota, we further investigated the niche characterization of microbial communities on red sandstone surface. According to Levins niche breadth theory, the distribution of microbiota composition can be used as an indicator of the environmental conditions[39]. Here, we calculated niche breadth (*Bcom*) and niche overlap (*Ocom*) as indicators to describe the habitat niche characterization of both bacteria and fungi making up the stone surface microbial communities. First, the *Bcom* was calculated with Levins index (Fig. 4 a-c). The results showed that the visually distinguishable microbial communities revealed decreased overall *Bcom* comparing with CK group. Such results were also further validated with Shannon index (Fig. S3 a-c). Then, the *Ocom* was calculated with Schoener index. The *Ocom* for both bacteria and fungi displayed a similar trend that CK samples revealed the highest *Ocom*, followed by Black, Green, and White, in descending order. All pairwise comparisons were statistically significant, indicating distinct niche overlaps among the different samples. When comparing *Ocom* across all samples, bacteria revealed a significantly higher *Ocom* than fungi (Fig. 4 d-f). Such results were also further validated with Pianka index (Fig. S3 d-f). In summary, both bacteria and fungi communities exhibit significant variations in *Bcom* and *Ocom* across different sample types (CK, Black, Green, White). In general, CK samples displayed widest niche breadth and highest overlap level compared with the rest groups of samples. These results suggested that the formation of visually distinguishable microbial communities on stone surface requires species to be more specialized, rather than relying on diverse and flexible species with metabolic flexibility and redundancy.

To further explore the inference, we also calculated the proportion of generalists and specialists among the microbial communities (Fig. 4 g-k). Generalists are species that are better suited to survive in diverse and challenging environments and often play pivotal roles within their communities. Specialists, on the other hand, have a more limited range of habitats and are specifically adapted to environmental conditions[40,41]. The results showed that at the ASVs level, the proportion of specialists in each type of sample was higher than that of generalists in both bacteria and fungi (Fig. 4 g). To determine whether there were differences between all bacteria and fungi, we also compared the proportion of specialists and generalists within these groups. The results showed that in each group of both bacteria and fungi, the proportion of specialists was higher than that of generalists. But, bacteria revealed overall higher proportion of generalists than that of specialists (Fig. 4 g). At the phylum level, up to 69.61 % of the bacteria were classified as the middle; the proportion of specialists (29.95 %) was higher than that of generalists (0.44 %) (Fig. 4 i, Table S5). Myxococcota revealed the largest fraction of specialists in bacteria (52.4%) among the top 10 dominant phyla. (Fig. 4 h, Table S5). For the fungi, 59.5% were classified as middle, 40.5% as specialists, and none of the ASV is classified as generalists. (Fig. 4 k, Table S6). This suggested that specialists prevail over generalists in the dominant phyla within the assembly of microbial communities. Notably, the non-dominant phyla (others) of both bacteria and fungi exhibited the highest proportion of specialists (Fig. 4 h, j; Table S5, S6). This suggested that the non-dominant phyla within the community might have even lower metabolic flexibility compared to the

dominant phyla.

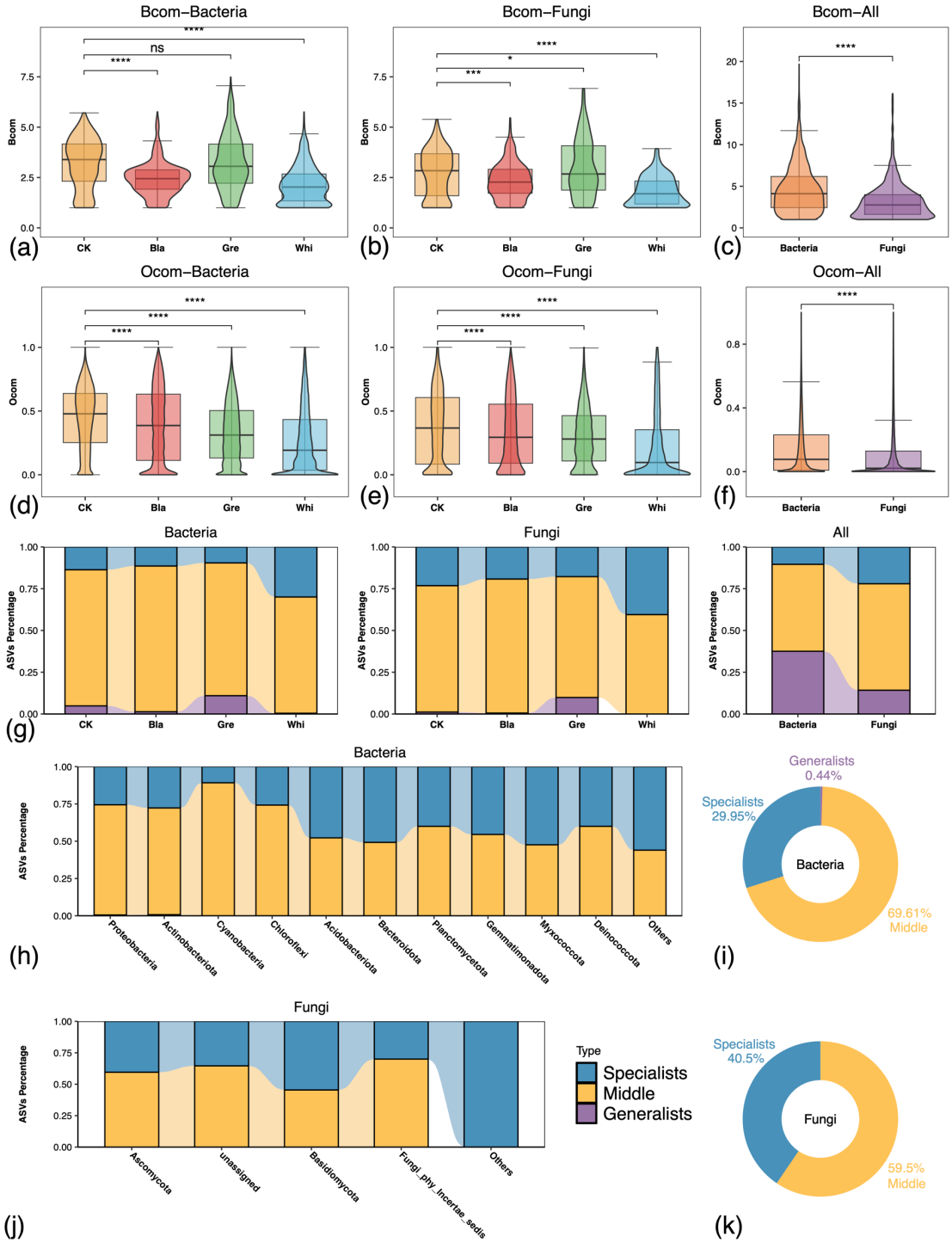


**Figure 4.** Niche characterization of the red sandstone surface microbial communities based on Levins niche breadth index and Schoener niche overlap index. (a). Average habitat niche breadth (*Bcom*) differences among three groups of bacteria samples comparing with CK in bacteria. (b). *Bcom* differences among three groups of fungi samples comparing with CK in fungi. (c). *Bcom* differences between bacteria and fungi. (d). Average habitat niche breadth (*Ocom*) differences among three groups of bacteria samples comparing with CK in bacteria. (e). Average *Ocom* differences among three groups of fungi samples comparing with CK in fungi. (f). Average *Ocom* differences between bacteria and fungi. (g). Proportional distribution of specialists, middle, and

generalists in each sample group, and between bacteria and fungi. (h). Proportional distribution of specialists, middle, and generalists of bacteria at phylum level based on Levins niche breadth index. (i). Overall proportion of the habitat niche breadth of bacteria at phylum level. (j). Proportional distribution of specialists, middle, and generalists of fungi at phylum level. (k). Overall proportion of the habitat niche breadth of fungi at phylum level. Notes: The *Bocm* was calculated with Levins index. The *Ocom* was calculated with Schoener index. All ASVs were defined as specialists, middle or generalists according to Levins niche breadth index. The asterisks in the boxplots stand for the significance of the Wilcoxon signed-rank test. The "ns" stands for no significance, single asterisk stands for $P < 0.05$, double asterisks stand for $P < 0.01$, Triple asterisks stand for $P < 0.001$, Four asterisks stand for $P < 0.0001$.

**2.4. Sparser network structure during the formation of visually distinguishable microbial communities on red sandstone surface**

Given the non-random assembly patterns observed in red sandstone surface microbial communities, we proceeded to construct microbial co-occurrence networks of both bacteria and fungi in different types of microbial communities to further explore the interaction patterns within these communities (Fig. 5). Subnetworks corresponding to each group were extracted from the global network constructed using all samples to obtain more robust group-specific networks.

Topological feature analysis revealed significant differences in bacterial networks among the different community types (Fig. 5a). Compared with the CK group, the three visually distinguishable microbial communities exhibited higher numbers of nodes and edges, which indicated that their formation was accompanied by a more complex bacterial association structure (Fig. 5a). However, in terms of structural parameters, the CK group showed higher clustering coefficient, degree centralization, edge density, and mean degree than the other three groups (Fig. 5b), which suggests that the visually distinguishable communities possessed a sparser local connectivity and overall network structure. Meanwhile, all three visually distinguishable communities exhibited lower proportions of negative correlations than CK, which implies that competitive or exclusionary interactions among bacterial members were reduced and replaced by more cooperative associations. The fungal networks showed a similar trend to the bacterial ones. The fungal networks of the three visually distinguishable communities underwent marked structural simplification, with fewer edges and reduced network density, which suggested weakened associations among fungal taxa (Fig. 5c, d). At the same time, the Black and Green groups displayed higher proportions of negative correlations than CK, which indicated enhanced antagonistic interactions among fungal members within the visually distinguishable communities (Fig. 5d). Overall, compared with CK, the microbial networks of the visually distinguishable communities became notably sparser in their connectivity.

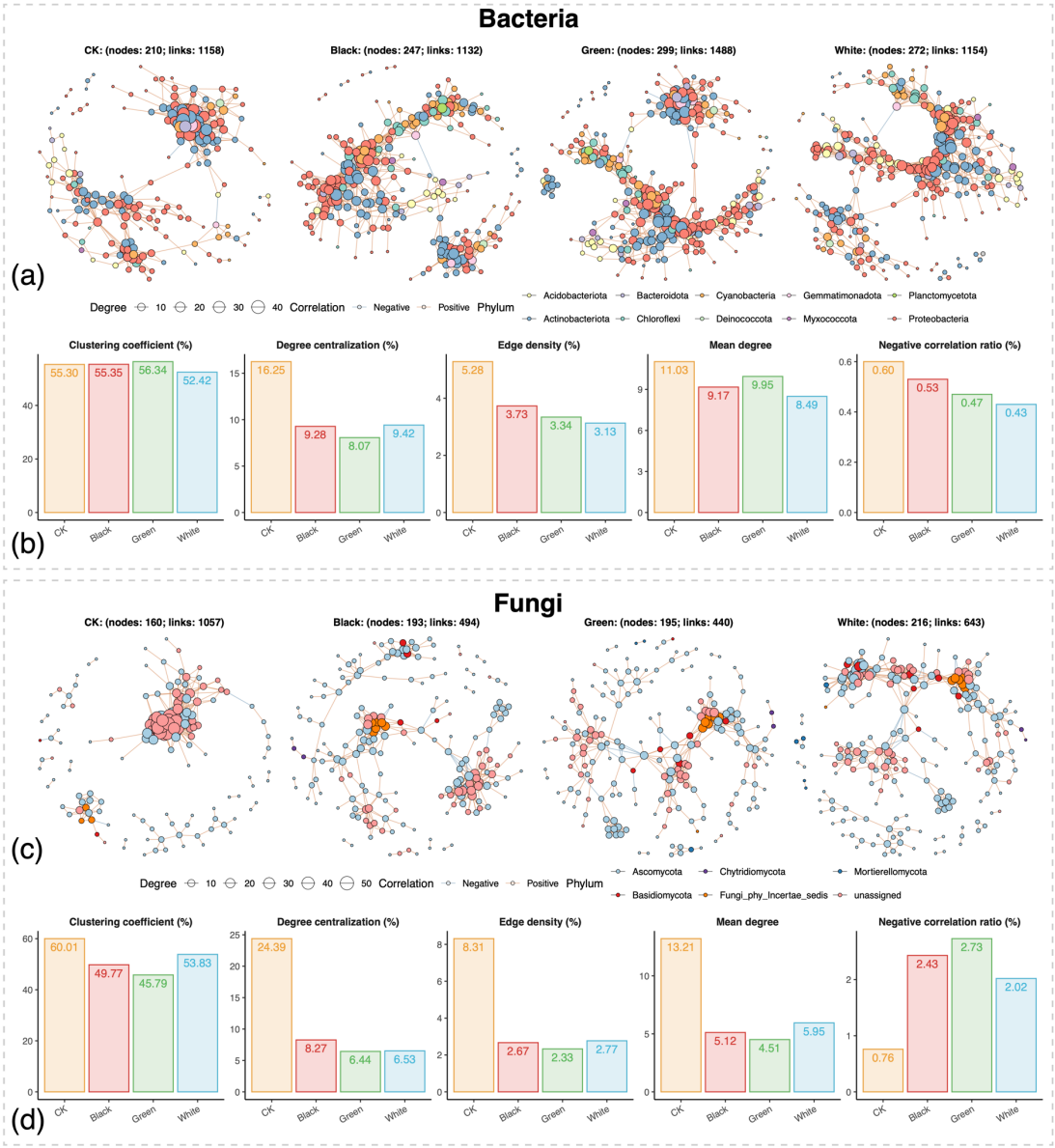


**Figure 5.** Topological features of the co-occurrence network within microbial communities on the stone surface. (a). Co-occurrence network of bacterial communities. (b). Topological comparisons of the four bacterial subnetworks. (c). Co-occurrence network of fungal communities. (d). Topological comparisons of the four fungal subnetworks. Notes: Subnetworks corresponding to each group were extracted from the global network constructed using all samples to obtain more robust group-specific networks.

### 2.5. Metabolic potential and nitrogen cycling of microbial communities on red sandstone surface

To elucidate the metabolic processes that enable the survival of microbial communities on the stone surface, we performed metagenomic sequencing for each type of microbial communities. Shotgun metagenomic sequencing generated approximately 9.6-13.2 Gb of raw data per sample. After quality control, 6.4-8.8 Gb of high-quality clean reads, comprising 206,491,166 clean reads in total, were retained for downstream analyses (Table S7).

Ten Gene Ontology (GO) terms that could potentially contribute to the assembly of microbial communities on red sandstone surface were identified in all four types of microbial communities[3].

These terms were associated with functions related to organism interactions, microbial survival, and trophic processes. Each of the ten GO terms was detectable in every group (Fig. 6 a).

Nitrogen cycle processes have been broadly reported as closely related with the deterioration of stone[3,9,42-44]. Hence, we performed detailed insight into nitrogen cycle processes. The results showed that nitrogen cycle related genes were widely present across all stone surface microbial communities (Fig. 6 b), indicating that these communities maintain the potential for nitrogen cycling even under extremely nutrient-limited and highly variable environmental conditions. Among all nitrogen cycle pathways, ammonium assimilation and nitrogen mineralization were the dominant processes, which account for about 38.52% and 31.39% of the total abundance of nitrogen cycle related reads, respectively (Fig. 6 c). This finding suggests active nitrogen exchange between microbial communities and the stone substrate. In addition, the relative abundance of nitrogen related genes varied among microbial communities of different color types (Fig. 6 c), which might reflect the effects of local microenvironmental heterogeneity on nutrient availability.

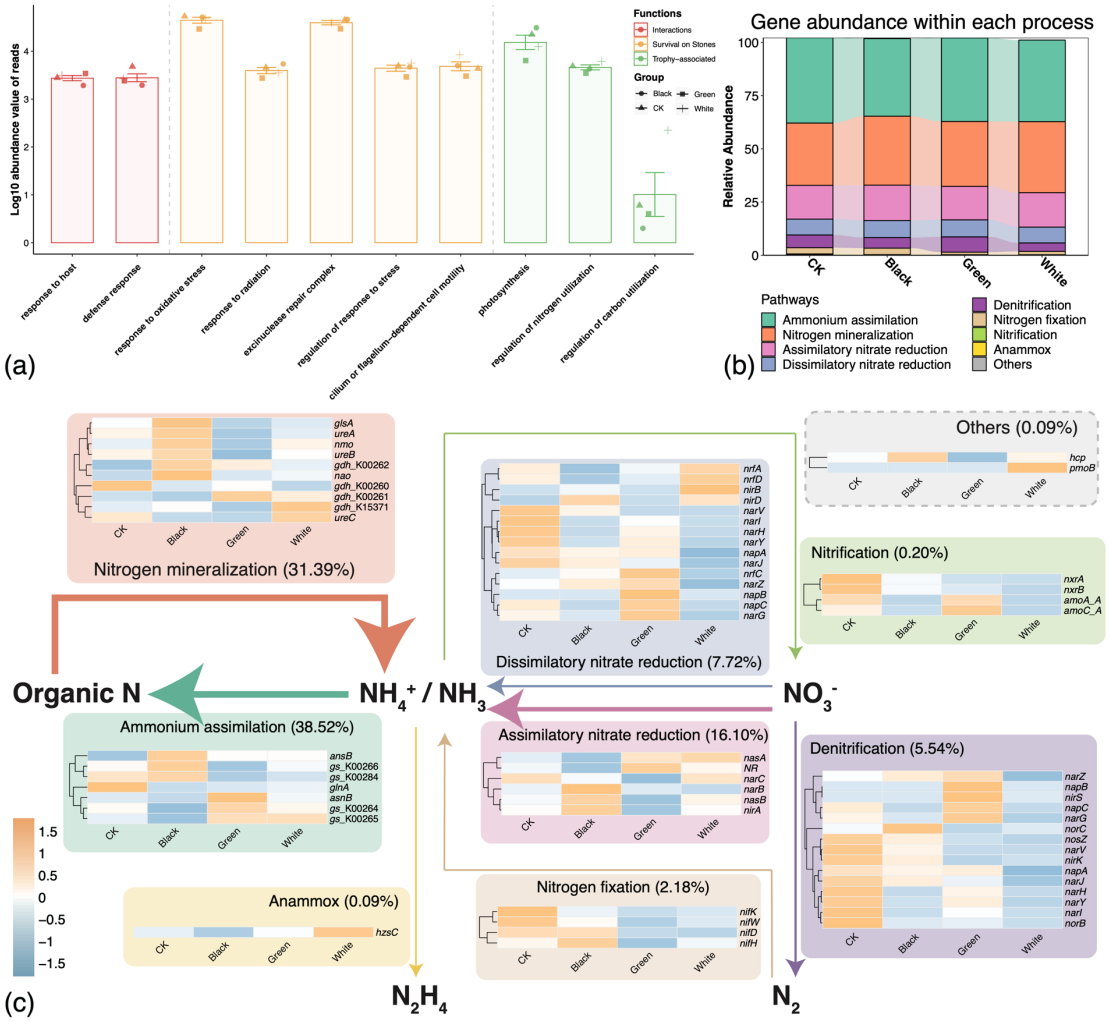


**Figure 6.** Functional profiles of the stone surface microbiota. (a). GO functional annotation of the stone surface microbiota. (b). Gene abundance within each nitrogen cycle pathway of the stone surface microbiota. (c). Nitrogen cycling potential of the stone surface microbiota. Arrow thickness corresponds to the proportion of functional genes for corresponding metabolic processes.

## 3. Discussion

310 Uncovering the diversity, assembly mechanisms, and functional traits of microbial
311 communities is a central focus in microbial ecology[18,45,46]. Recently, the role of microbial
312 communities on stone surfaces has garnered increasing attention, particularly in the field of stone
313 cultural heritage conservation[47]. In this study, we present a pioneering case study on the ecological
314 roles of microbiota on red sandstone surface, using the Leshan Giant Buddha as an example. The
315 results indicate that the taxonomic composition of microbial communities varies according to their
316 coloration. During the formation of visually distinguishable microbial communities, core metabolic
317 pathways of microbial communities were maintained but gene profiles varied across different
318 types of microbial communities, particularly in nitrogen cycle-related biogeochemical processes.
319 Dispersal limitation and heterogeneous selection dominate the assembly of stone surface
320 microbial communities. Habitat specialists play a more significant role than generalists during the
321 formation of microbial communities on the red sandstone surface. As visible microbial
322 communities form on stone surface, network complexity increases, and resistance to disturbances
323 is enhanced. By comparing our findings with previous studies on microbial communities on stone
324 surface, we inferred the following commonalities and unique characteristics in the ecological
325 features of stone surface microbial communities.
326
327 **3.1. Conservation of core ecological functions under harsh stone surface conditions**
328 In this study, the microbial diversity analysis revealed that Proteobacteria, Actinobacteria,
329 Cyanobacteria, Chloroflexi, and Acidobacteriota dominate the top phyla among the bacteria in all
330 samples, while Ascomycota stands as the most dominant phylum in fungi, despite the distinct
331 microbial community morphology across different sample groups. These phylum-level diversity
332 patterns are largely consistent with previous reports on taxonomic diversity of microbial
333 communities on the surface of other stone types. However, significant differences were observed
334 at the genus level[2-4,35,48-50]. These variations might be attributed to site-specific factors, including
335 the local climate and the type of stone cultural heritage[51]. Comparison with previous studies
336 suggests that core ecological functions of stone surface microbes are conserved across the surfaces
337 of various types of stone. The capability to withstand pressures such as fluctuations between wet
338 and dry conditions, endure UV stress on stone surface, and facilitate ion exchange with the stone
339 appears essential for the persistence of microbial communities on the outdoor stone surface[3,9].
340 The nitrogen cycle is likely a conserved and essential pathway that mediates ion exchange
341 between microbial communities and the stone substrate across various types of stone surface
342 ecosystems. This study revealed that distinct microbial communities exhibited similar ecological
343 functional patterns, which highlights the important role of functional redundancy in maintaining
344 the stability of stone surface ecosystems. Dispersal limitation and environmental filtering jointly
345 shaped the taxonomic divergence among communities, while the core nitrogen cycling functions
346 were likely sustained through complementary metabolic strategies. These findings further support
347 that the nitrogen cycle serves as a crucial pathway for ion exchange between microbial
348 communities and the stone substrate, regardless of taxonomic convergence or divergence. For
349 example, previous study reported that the two dominated types of nitrogen cycling genes in
350 limestone surface microbial communities are nitrogen assimilation and mineralization, which is
351 coherent with what we found in red sandstone surface microbial communities in this study[3].
352 Nitrifying bacteria genera *Nitrospira* and *Nitrosomonas* were significantly enriched in limestone
353 surface microbial communities[3]. In another case study involving regular sandstone, *Nitrosopumilus*

354 and *Nitrospira* were also identified from deteriorated sediments[9]. Furthermore, *Methylobacterium*,
355 another dominant genus identified in our study, comprises species recognized as plant growth-
356 promoting rhizobacteria, with genomes encoding enzymes involved in nitrogen metabolism and
357 ammonia assimilation[52]. Despite the overall functional convergence of nitrogen metabolism,
358 differences in the relative abundance and composition of nitrogen cycling genes were observed
359 among microbial communities of different color types. These variations likely reflect the
360 microenvironmental heterogeneity of the stone surface, where factors such as moisture, organic
361 matter, and light gradients influence nutrient availability and redox conditions[53]. Consequently,
362 environmental filtering and niche specialization may have selected for distinct microbial taxa with
363 complementary nitrogen transformation capabilities. Such taxon-specific metabolic adaptations
364 could explain the observed diversity of nitrogen-related genes while maintaining overall functional
365 redundancy within the system.
366 Conserved core functions among microbial communities within similar niches are not unique
367 to microbial communities on stone surface. For example, several gut microbiota studies have
368 reported functional, but not compositional, convergence of gut microbiomes[54-57]. Some soil
369 microbiota studies also reported the stable functional structure despite high taxonomic
370 variability[58-60]. In addition, microbial functional genes of ocean microbiota that execute certain
371 functions, such as $B_{12}$ biosynthesis, are widely distributed, while the microbial taxa that carry these
372 genes vary significantly[61]. These results corroborate the ecological hypothesis that environment
373 truly selects for function, rather than taxonomy[62]. Different taxonomic groups could reveal
374 convergent functions as a result of functional redundancy among microbial systems[63]. On stone
375 surface, conserved core functions among various types of stones might be attributed to the
376 selective pressure imposed by the harsh living conditions on the stone surface, favoring the survival
377 of microbial communities with specific functions[58,64-66].
378
379 **3.2. Assembly of stone surface microbial communities requires a general pattern of dynamic**
380 **interactions**
381 In this study, we witnessed the extensive microbe-microbe and microbe-environment
382 interactions within the microbial communities on the stone surface. The mutual effect of
383 heterogeneous selection and dispersal limitation controls the assembly processes of both bacterial
384 and fungal communities on the red sandstone surface. Such results differ from previous studies on
385 the assembly processes of microbial communities on limestone surface, where the assembly
386 processes are driven by homogeneous selection and dispersal limitation[3]. This suggests that the
387 assembly mechanisms of microbial communities on stone surface might vary based on stone types,
388 geographical locations, climatic characteristics, or other environmental factors. In addition, the
389 results of the DOC model analysis suggest a general pattern of dynamic interspecific interactions
390 within the communities on the red sandstone surface and high selective pressure on the red
391 sandstone surface[28,67-69]. Such complexity was further testified in this study by the topological
392 feature analysis of the microbial networks. The active biogeochemical metabolism such as
393 ammonium assimilation and nitrogen mineralization processes by the microbial communities also
394 suggests their active interactions with the red sandstone substrate[70]. The elevated complexity of
395 microbial communities might arise from widely functional complementarity and the resulting
396 extensive interactions among microbes[71].
397 Here, we propose a hypothesis that a possible model capable of precisely interpreting the

assembly processes of stone surface microbial communities is the classic MacArthur consumer-resource model, where species-species interactions are mediated through resource dynamics[72-74]. Because of the nutrient-limited nature of the stone surface, the colonization by pioneer species is primarily driven by deterministic processes linked to nutrient availability, which aligns with commonly observed among natural communities from various locations[75]. Some pioneer species utilize inorganic energy from the stone to establish themselves. These species then leak metabolic by-products into the environment, increasing the diversity of resources and enhancing the biocompatibility of the stone surface. Other species can subsequently utilize these leaked metabolites, in turn releasing new by-products into the environment, further enhancing the biocompatibility of the stone surface, and facilitating the formation of microbial communities. The observed decrease in ecological niche breadth among the visually distinguishable microbial communities in this study also suggests that the utilization of specific resources is more efficient within these communities. We also observed that specialization prevails over flexibility during the formation of microbial communities on red sandstone surface. This is consistent with a previous study on the assembly of microbial communities in a wide range of well-defined resource environments, where habitat specialists also drive the increase of diversity in such microbial communities[19]. Meanwhile, the sparser structure during the formation of the visually distinguishable microbial networks suggests that although the communities are taxonomically diverse, their members are relatively independent or show clear functional differentiation. The reduction in network interactions, especially for fungal communities, indicates that each species occupies a more defined ecological niche within the biofilm, with stronger resource competition or spatial segregation. It can therefore be inferred that different modules within the microbial community might form a micro-ecological isolation, which allows various microbial populations to coexist through spatial and functional differentiation. Such spatial partitioning might occur between the surface and deeper layers of the microbial community. Future research should make more detailed spatial distinctions between surface and subsurface layers and within them to better resolve the mechanisms of community formation. In addition, higher-resolution temporal studies are needed to clarify the dynamic processes underlying microbial community assembly.

### 3.3. Summary

In summary, this study investigated the ecological and functional characteristics of microbial communities on the red sandstone surface of the Leshan Giant Buddha. Under the interplay of dispersal limitation and heterogeneous selection, the microbiota on the red sandstone were assembled into distinct types of visually distinguishable microbial communities, which significantly differed in the taxonomic composition of these communities. However, under the harsh habitat on red sandstone surface, such as UV radiation, fluctuations between dry and wet conditions, and limited nutrient availability, the core functions of the microbe across different types of microbial communities are conserved. These functions are particularly enriched in biogeochemical processes related to nitrogen cycling and responses to environmental stress. The formation of visually distinguishable microbial communities is associated with a narrower niche width, a higher proportion of habitat specialists, and a sparser network structure (Fig. 7). Given the nutrient limitations of the red sandstone surface, the classic MacArthur consumer-resource model might provide a potential framework to further explain the assembly mechanisms of these microbial communities. In the future, in-depth temporal and spatial studies of the ecological characteristics

and functional potential of these microbial communities will provide valuable insights into their assembly on red sandstone surfaces. Moreover, microbial deterioration affects not only stone cultural heritage but also a wide range of other cultural heritage materials[76-80]. The microbial ecology-based approach used in this study will help advance research on microbial deterioration mechanisms in other cultural heritage materials, providing a model for future work.

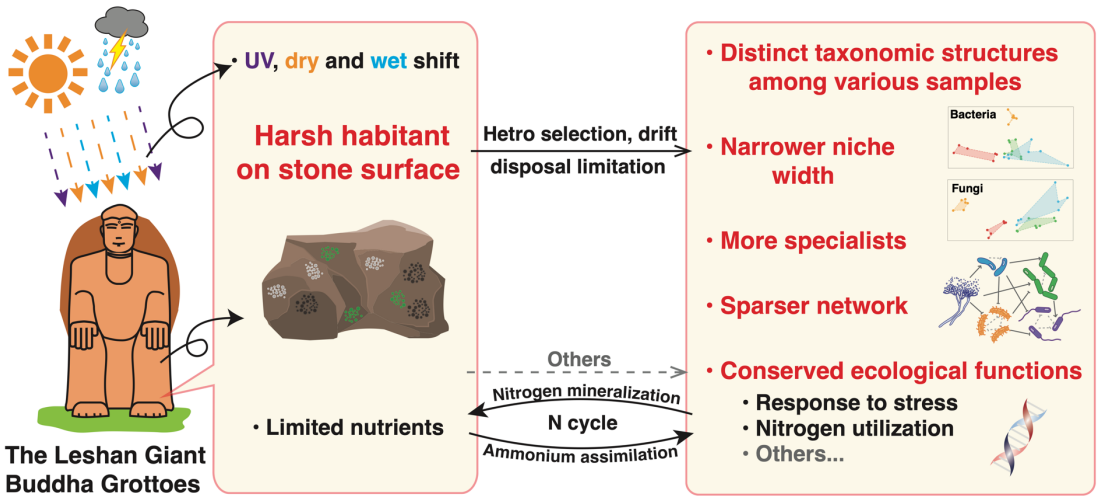


**Figure 7.** Schematic diagram illustrates the characteristics of microbial communities on the red sandstone surface of the Leshan Giant Buddha

## 4. Materials and Methods

### 4.1. Sampling processes

The Leshan Giant Buddha is a world-famous, typical red sandstone-made, UNESCO World Heritage site. It was built between 713 and 803 during the Tang dynasty, located in the Leshan city, Sichuan province, China. Samples used in this study were collected from the stone surface of the Leshan Giant Buddha between 2019 and 2022. Among these, 6 samples have been used in our previous study[35]. The other 21 samples were newly collected in 2022. Surface samples were scraped using a pre-cleaned steel scalpel and then stored in low temperature until DNA extraction.

### 4.2. DNA extraction and NGS sequencing

The DNA extraction was applied using a genomic DNA extraction kit from TIANGEN (DP302-02) with 0.5 g of sample processed for extraction. The amplicon sequencing was performed as followed. The 16S V3-V4 region rDNA and ITS2 region were amplified by PCR (initial denaturation at 98 ℃ for 30 seconds; 32cycles of denaturation at 98 ℃ for 10 seconds, annealing at 54℃ for 30 seconds, and extension at 72 ℃ for 45 seconds; and then final extension at 72 ℃ for 10 minutes.) with following primers: 0341-F (CCT ACG GGN GGC WGC AG) and 806-R (GAC TAC HVG GGT ATC TAA TCC) for 16S[81], ITS1FI2 (GTG ART CAT CGA ATC TTT G) and ITS2 (TCC TCC GCT TAT TGA TAT GC) for ITS2. The PCR products were purified by AMPure XT beads (Beckman Coulter Genomics, Danvers, MA, USA) and quantified by Qubit (Invitrogen, USA). The amplicon pools were prepared for sequencing and the size and quantity of the amplicon library were assessed on Agilent 2100 Bioanalyzer (Agilent, USA) and with the Library Quantification Kit for Illumina (Kapa Biosciences,

473 Woburn, MA, USA), respectively, and then sequenced on Illumina NovaSeq 6000 PE250 platform
474 in LC-Bio Technology Co., Ltd, Hang Zhou, Zhejiang Province, China. The raw sequence data were
475 then deposited in the Genome Sequence Archive[82] in National Genomics Data Center[83], China
476 National Center for Bioinformation / Beijing Institute of Genomics, Chinese Academy of Sciences
477 (GSA: CRA013382) that are publicly accessible at https://ngdc.cncb.ac.cn/gsa.
478 The DNA libraries were sequenced on the illumina NovaseqTM 6000 platform by LC Bio
479 Technology CO., Ltd (Hangzhou, China). We are grateful to LC Bio Technology CO., Ltd for assisting
480 in sequencing. DNA concentration was measured using Qubit. Based on the measured
481 concentration, equal-mass DNA samples were pooled from all samples within each group by mixing
482 100 ng of DNA from each sample. The metagenome sequencing was performed as followed: DNA
483 library was constructed by TruSeq Nano DNA LT Library Preparation Kit (FC-121-4001). DNA was
484 fragmented by dsDNA Fragmentase (NEB, M0348S) by incubate at 37°C for 30min. Library
485 construction begins with fragmented cDNA. Blunt-end DNA fragments are generated using a
486 combination of fill-in reactions and exonuclease activity, and size selection is performed with
487 provided sample purification beads. An A-base is then added to the blunt ends of each strand,
488 preparing them for ligation to the indexed adapters. Each adapter contains a T-base overhang for
489 ligating the adapter to the A-tailed fragmented DNA. These adapters contain the full complement
490 of sequencing primer hybridization sites for single, paired-end, and indexed reads. Single- or dual-
491 index adapters are ligated to the fragments and the ligated products are amplified with PCR. The
492 raw sequence data were then deposited in the Genome Sequence Archive[82] in National Genomics
493 Data Center[83], China National Center for Bioinformation / Beijing Institute of Genomics, Chinese
494 Academy of Sciences (GSA: CRA013393) that are publicly accessible at https://ngdc.cncb.ac.cn/gsa.
495
496 **4.3. Taxonomic and functional annotations**
497 For the amplicon sequencing data, the DADA2 R package[84] in QIIME 2[85] was used to conduct
498 a complete pipeline to generate raw paired-end fastq sequencing files into merged, denoised,
499 chimera-free sequences and output ASV. The ASV tables for both 16S and ITS were rarified to a
500 minimum sequencing depth (13,622 for 16S and 16,232 for ITS) to mitigate the impact of
501 sequencing depth on subsequent analysis. Representative ASV sequences were classified into
502 different organisms using a naive Bayesian model with RDP classifier[86], which is based on the SILVA
503 database[87] (version 138) for 16S or UNITE database[88] (version 9.0) for ITS.
504 Metagenome raw sequencing reads were processed to obtain valid reads for further analysis.
505 First, sequencing adapters were removed from sequencing reads using cutadapt (version 1.9).
506 Secondly, low quality reads were trimmed by fqtrim (version 0.94) using a sliding-window
507 algorithm. Window size is 6 bp, and base quality must not be lower than 20. Once quality-filtered
508 reads were obtained, they were de novo assembled to construct the metagenome for each sample
509 by MEGAHIT with the following parameters: *--k-list 21,29,39,59,79,99,119,141 -m 0.8 -t 8 --min-*
510 *contig-len 200 --continue*. All coding regions (CDS) of metagenomic contigs were predicted by
511 MetaGeneMark (version 3.26). CDS sequences of all samples were clustered by CD-HIT (version
512 4.6.1)[89] to obtain unigenes with the following parameters: *-c 0.95 -aS 0.9 -d 0 -g 1 -M 20000 -T 20*.
513 The CDS sequences from all samples are clustered together to group highly similar or identical
514 sequences, and a single representative sequence from each cluster is chosen as a unigene. Unigene
515 abundance for a certain sample were estimated by TPM based on the number of aligned reads by
516 bowtie2 (version 2.2.0)[90]. The TPM value for each Unigene was calculated by dividing its RPK (Reads

517 Per Kilobase) by the sum of RPK values across all Unigenes in the sample, then multiplying the
518 result by 1,000,000 to normalize expression levels to a per-million scale. The functional annotations
519 (GO, KEGG) of unigenes were obtained by aligning them against the NCBI NR database (version
520 20191121) by DIAMOND (version 0.9.14)[91] with the following parameters: *-k 25 -e 0.00001 --query-*
521 *cover 0 --min-score 0 --id 0.* Nitrogen cycling genes were annotated with the NCycDB database[92].
522 Heatmaps were visualized with pheatmap package in R.
523 The figures in this study was widely plotted in R project ggplot2 package[93]. Top 10 phyla were
524 visualized in R with ggplot2 and ggalluvial as our previous publications[69,76]. Bray-Curtis distance
525 matrix was calculated in R with Vegan package[94] (version 2.5.7). NMDS was then generated with
526 Vegan and plotted with ggplot2 package. Adonis and anosim test were used to calculate the
527 significance of β diversity differences.
528
529 **4.4. Microbial communities assembly analyses**
530 The DOC model was used to determine whether microbiota on the red sandstone surface of
531 the Leshan Giant Buddha have unique ecological dynamics in R with DOC package
532 (https://github.com/Russel88/DOC) according to previous reports[3,68,69]. The DOC was obtained by
533 plotting the dissimilarity (Jensen–Shannon divergence) against the overlap fraction of taxa for each
534 pairwise community[28] with 1000 bootstrap replicates to evaluate the significance and initiation of
535 negative slopes.
536 Null model analysis was performed as described by Stegen *et al*. [37,38] and visualized as
537 previous research[69]. The deviation of phylogenetic and taxonomic diversity was estimated with
538 999 randomizations. Beta mean nearest taxon distance (βMNTD) and beta nearest taxon index
539 (βNTI) were calculated with picante package in R[95]. Phylogenetic analysis were performed by
540 iqtree2 with 1000 bootstrap[96]. A significant deviation indicated the dominance of deterministic
541 processes, including homogeneous or heterogeneous selection processes when βNTI < −2 or βNTI >
542 2, respectively. The Bray-Curtis based Raup-Crick (RCbray), the deviation between Bray-Curtis and
543 the null distribution, was then calculated to partition pairwise comparisons that assigned the
544 stochastic processes when |βNTI| < 2. The relative influence of homogenizing dispersal and
545 dispersal limitation was quantified as the fraction of pairwise comparisons with RCbray < −0.95
546 and RCbray > 0.95, respectively. In addition, dispersal was seen as stochastic processes in this
547 research, not restricted to deterministic or stochastic processes as previously described[3,18]. Low-
548 occurrence ASVs with a prevalence less than 50% and low abundance ASVs with total read counts
549 lower than the number of samples were excluded to ensure the accuracy in taxon-specific assembly
550 characterization and reduce type I errors as presented in previous research[3,69].
551
552 **4.5. Niche characteristics analysis**
553 Levins niche breadth index, Shannon niche breadth index, Schoener niche overlap index, and
554 Pianka niche overlap index were calculated with spaa package in R[97]. Generalists were defined by
555 ASVs with *Bcom* > 5, whereas specialists were defined by those with *Bcom* < 1.5[3,98]. Significance of
556 the differences was tested by Wilcoxon signed-rank test.
557
558 **4.6. Network construction and topological feature analysis**
559 To obtain more robust group-specific networks, subnetworks corresponding to each group
560 were extracted from the global network constructed using all samples. Microbial co-occurrence

networks were constructed according to previous publication[99] with modifications by ggClusterNet R package[100]. To reduce noise from rare taxa, only the top 400 most abundant ASVs across all samples were retained for network analysis. Pairwise correlations between ASVs were calculated using the Spearman's rank correlation coefficient. A correlation coefficient threshold of $|r| > 0.75$ and P values $< 0.001$ were retained for network construction to ensure significant and robust associations. Group-specific subnetworks were derived by retaining ASVs with nonzero abundance that appeared in the global network and were not isolated within the extracted subnetwork, along with their edges. The subnetworks were then visualized with ggraph in R[101]. Network topology metrics of each subnetwork were computed with the igraph package in R[102].

### 4.7. Acknowledgements of English edition

During the preparation of this work the authors used ChatGPT in order to check the English grammar. After using this tool, the authors reviewed and edited the content as needed and take full responsibility for the content of the publication.

## Availability of data and materials

The raw sequence data reported in this paper have been deposited in the Genome Sequence Archive in National Genomics Data Center, China National Center for Bioinformation / Beijing Institute of Genomics, Chinese Academy of Sciences (GSA: CRA013382 & GSA: CRA013393) that are publicly accessible at https://ngdc.cncb.ac.cn/gsa.

All scripts used in this study are publicly available at the GitHub repository (https://github.com/Bowenw6/Microbiome_Buddha_Grotto_2023).

## Author Contributions Statement

**Bowen Wang**: Conceptualization, Data curation, Formal analysis, Investigation, Methodology, Resources, Visualization, Writing - Original Draft, Writing - Review & Editing. **Chengshuai Zhu**: Conceptualization, Data curation, Investigation, Resources. **Xin Wang**: Conceptualization, Investigation, Resources. **Tianyu Yang**: Conceptualization, Investigation, Resources. **Bingjian Zhang**: Conceptualization, Funding acquisition, Supervision. **Yulan Hu**: Conceptualization, Funding acquisition, Project administration, Supervision, Writing - Review & Editing.

## Competing interests

No, we declare that the authors have no competing interests, or other interests that might be perceived to influence the results and/or discussion reported in this paper.

## Funding

This work is supported by the National Key Research and Development Program (2019YFC1520503)

601
602
603 **References:**
604
605 1 Liu, X. B., Koestler, R. J., Warscheid, T., Katayama, Y. & Gu, J. D. Microbial deterioration and
606 sustainable conservation of stone monuments and buildings. *Nat Sustain* **3**, 991-1004 (2020).
607 https://doi.org/10.1038/s41893-020-00602-5
608 2 Brewer, T. E. & Fierer, N. Tales from the tomb: the microbial ecology of exposed rock surfaces.
609 *Environ Microbiol* **20**, 958-970 (2018). https://doi.org/10.1111/1462-2920.14024
610 3 He, J. *et al.* From surviving to thriving, the assembly processes of microbial communities in
611 stone biodeterioration: A case study of the West Lake UNESCO World Heritage area in China.
612 *Sci Total Environ* **805**, 150395 (2022). https://doi.org/10.1016/j.scitotenv.2021.150395
613 4 Qiang, L., Zhang, B. B., Yang, B. X. & Ged, C. Q. Deterioration-Associated Microbiome of Stone
614 Monuments: Structure, Variation, and Assembly. *Appl Environ Microbiol* **84**, e02680-02617-
615 02617 (2018).
616 5 Li, T., Hu, Y. & Zhang, B. Biomineralization Induced by Colletotrichum acutatum: A Potential
617 Strategy for Cultural Relic Bioprotection. *Front Microbiol* **9**, 1884 (2018).
618 6 Jroundi, F., Gonzalez-Muñoz, M. T. & Rodriguez-Navarro, C. in *Microorganisms in the*
619 *Deterioration and Preservation of Cultural Heritage* (ed Edith Joseph) 281-299 (Springer
620 International Publishing, 2021).
621 7 Liu, X. *et al.* Biofilms on stone monuments: biodeterioration or bioprotection? *Trends Microbiol*
622 **30**, 816-819 (2022). https://doi.org/https://doi.org/10.1016/j.tim.2022.05.012
623 8 Li, J. *et al.* The active microbes and biochemical processes contributing to deterioration of
624 Angkor sandstone monuments under the tropical climate in Cambodia – A review. *J Cult Herit*
625 **47**, 218-226 (2021). https://doi.org/https://doi.org/10.1016/j.culher.2020.10.010
626 9 Ding, X. *et al.* Microbiome and nitrate removal processes by microorganisms on the ancient
627 Preah Vihear temple of Cambodia revealed by metagenomics and N-15 isotope analyses. *Appl*
628 *Microbiol Biotechnol* **104**, 9823-9837 (2020). https://doi.org/10.1007/s00253-020-10886-4
629 10 Wu, F. *et al.* Metagenomic and metaproteomic insights into the microbiome and the key
630 geobiochemical potentials on the sandstone of rock-hewn Beishiku Temple in Northwest China.
631 *Sci Total Environ* **893**, 164616 (2023).
632 https://doi.org/https://doi.org/10.1016/j.scitotenv.2023.164616
633 11 Fidanza, M. R. & Caneva, G. Natural biocides for the conservation of stone cultural heritage: A
634 review. *J Cult Herit* **38**, 271-286 (2019).
635 https://doi.org/https://doi.org/10.1016/j.culher.2019.01.005
636 12 Li, Q., Wu, C., He, J. & Zhang, B. Unraveling the microbiotas and key genetic contexts identified
637 on stone heritage using illumina and nanopore sequencing platforms. *Int Biodeter Biodegr* **185**,
638 105688 (2023). https://doi.org/https://doi.org/10.1016/j.ibiod.2023.105688
639 13 Ding, X. *et al.* Microbiome characteristics and the key biochemical reactions identified on stone
640 world cultural heritage under different climate conditions. *Journal of Environmental*
641 *Management* **302**, 114041 (2022).
642 https://doi.org/https://doi.org/10.1016/j.jenvman.2021.114041
643 14 Ennis, N. J., Dharumaduri, D., Bryce, J. G. & Tisa, L. S. Metagenome Across a Geochemical
644 Gradient of Indian Stone Ruins Found at Historic Sites in Tamil Nadu, India. *Microb Ecol* **81**, 385-

395 (2021). https://doi.org/10.1007/s00248-020-01598-3

15 Louati, M. *et al.* Elucidating the ecological networks in stone-dwelling microbiomes. *Environ Microbiol* **22**, 1467-1480 (2020). https://doi.org/https://doi.org/10.1111/1462-2920.14700

16 Li, T., Cai, Y. & Ma, Q. Microbial Diversity on the Surface of Historical Monuments in Lingyan Temple, Jinan, China. *Microb Ecol* (2022). https://doi.org/10.1007/s00248-021-01955-w

17 Cattò, C. *et al.* Biofilm colonization of stone materials from an Australian outdoor sculpture: Importance of geometry and exposure. *Journal of Environmental Management* **339**, 117948 (2023). https://doi.org/https://doi.org/10.1016/j.jenvman.2023.117948

18 Zhou, J. & Ning, D. Stochastic Community Assembly: Does It Matter in Microbial Ecology? *MMBR* **81**, e00002-00017 (2017). https://doi.org/10.1128/MMBR.00002-17

19 Dal Bello, M., Lee, H., Goyal, A. & Gore, J. Resource–diversity relationships in bacterial communities reflect the network structure of microbial metabolism. *Nature Ecology & Evolution* **5**, 1424-1434 (2021). https://doi.org/10.1038/s41559-021-01535-8

20 Goldford, J. E. *et al.* Emergent simplicity in microbial community assembly. *Science* **361**, 469-474 (2018). https://doi.org/10.1126/science.aat1168

21 Ning, D. *et al.* A quantitative framework reveals ecological drivers of grassland microbial community assembly in response to warming. *Nat Commun* **11**, 4717 (2020). https://doi.org/10.1038/s41467-020-18560-z

22 Chase, J. M. Stochastic Community Assembly Causes Higher Biodiversity in More Productive Environments. *Science* **328**, 1388-1391 (2010). https://doi.org/10.1126/science.1187820

23 Ofiţeru, I. D. *et al.* Combined niche and neutral effects in a microbial wastewater treatment community. *PNAS* **107**, 15345-15350 (2010). https://doi.org/10.1073/pnas.1000604107

24 Chesson, P. Mechanisms of Maintenance of Species Diversity. *Annual Review of Ecology, Evolution, and Systematics* **31**, 343-366 (2000). https://doi.org/https://doi.org/10.1146/annurev.ecolsys.31.1.343

25 Fargione, J., Brown, C. S. & Tilman, D. Community assembly and invasion: An experimental test of neutral versus niche processes. *PNAS* **100**, 8916-8920 (2003). https://doi.org/10.1073/pnas.1033107100

26 Chave, J. Neutral theory and community ecology. *Ecol Lett* **7**, 241-253 (2004). https://doi.org/https://doi.org/10.1111/j.1461-0248.2003.00566.x

27 Vega, N. M. & Gore, J. Stochastic assembly produces heterogeneous communities in the Caenorhabditis elegans intestine. *PLOS Biology* **15**, e2000633 (2017). https://doi.org/10.1371/journal.pbio.2000633

28 Bashan, A. *et al.* Universality of human microbial dynamics. *Nature* **534**, 259-262 (2016). https://doi.org/10.1038/nature18301

29 Ning, D. *et al.* Environmental stress mediates groundwater microbial community assembly. *Nature Microbiology* **9**, 490-501 (2024). https://doi.org/10.1038/s41564-023-01573-x

30 He, Q. *et al.* Temperature and microbial interactions drive the deterministic assembly processes in sediments of hot springs. *Sci Total Environ* **772**, 145465 (2021). https://doi.org/https://doi.org/10.1016/j.scitotenv.2021.145465

31 Tolkkinen, M. *et al.* Multi-stressor impacts on fungal diversity and ecosystem functions in streams: natural vs. anthropogenic stress. *Ecology* **96**, 672-683 (2015). https://doi.org/https://doi.org/10.1890/14-0743.1

32 Huot, O. B. & Tamborindeguy, C. Drought stress affects olanum lycopersicum susceptibility to

689 actericera cockerelli colonization. *Entomologia Experimentalis et Applicata* **165**, 70-82 (2017).
690 https://doi.org/https://doi.org/10.1111/eea.12627
691 33 Luo, C., Lü, F., Shao, L. & He, P. Application of eco-compatible biochar in anaerobic digestion to
692 relieve acid stress and promote the selective colonization of functional microbes. *Water Res*
693 **68**, 710-718 (2015). https://doi.org/https://doi.org/10.1016/j.watres.2014.10.052
694 34 Bai, F. *et al.* Microbial biofilms on a giant monolithic statue of Buddha: The symbiosis of
695 microorganisms and mosses and implications for bioweathering. *Int Biodeter Biodegr* **156**
696 (2021). https://doi.org/ARTN 105106 10.1016/j.ibiod.2020.105106
697 35 Zhu, C. *et al.* Analysis of the Microbiomes on Two Cultural Heritage Sites. *Geomicrobiol J*, 1-10
698 (2022). https://doi.org/10.1080/01490451.2022.2137604
699 36 Zhu, C. *et al.* Unveiling the dual role of biocolonization: a case study on the deterioration and
700 preservation of sandstone monuments in Leshan Giant Buddha, China. *World Journal of*
701 *Microbiology and Biotechnology* **41**, 25 (2025). https://doi.org/10.1007/s11274-024-04237-y
702 37 Stegen, J. C., Lin, X., Konopka, A. E. & Fredrickson, J. K. Stochastic and deterministic assembly
703 processes in subsurface microbial communities. *ISME J* **6**, 1653-1664 (2012).
704 https://doi.org/10.1038/ismej.2012.22
705 38 Stegen, J. C. *et al.* Quantifying community assembly processes and identifying features that
706 impose them. *ISME J* **7**, 2069-2079 (2013). https://doi.org/10.1038/ismej.2013.93
707 39 Levins, R. *Evolution in Changing Environments Some Theoretical Explorations. (MPB-2)*.
708 (Princeton University Press, 1968).
709 40 Sexton, J. P., Montiel, J., Shay, J. E., Stephens, M. R. & Slatyer, R. A. Evolution of Ecological Niche
710 Breadth. *Annual Review of Ecology, Evolution, and Systematics* **48**, 183-206 (2017).
711 https://doi.org/10.1146/annurev-ecolsys-110316-023003
712 41 von Meijenfeldt, F. A. B., Hogeweg, P. & Dutilh, B. E. A social niche breadth score reveals niche
713 range strategies of generalists and specialists. *Nature Ecology & Evolution* **7**, 768-781 (2023).
714 https://doi.org/10.1038/s41559-023-02027-7
715 42 Meng, H., Zhang, X., Katayama, Y., Ge, Q. & Gu, J.-D. Microbial diversity and composition of the
716 Preah Vihear temple in Cambodia by high-throughput sequencing based on genomic DNA and
717 RNA. *Int Biodeter Biodegr* **149** (2020).
718 43 Meng, S. *et al.* Community structures and biodeterioration processes of epilithic biofilms imply
719 the significance of micro-environments. *Sci Total Environ* **876**, 162665 (2023).
720 https://doi.org/https://doi.org/10.1016/j.scitotenv.2023.162665
721 44 Chen, X. *et al.* The Organisms on Rock Cultural Heritages: Growth and Weathering. *Geoheritage*
722 **13** (2021). https://doi.org/ARTN 5610.1007/s12371-021-00588-2
723 45 Escalas, A. *et al.* Microbial functional diversity: From concepts to applications. *Ecology and*
724 *Evolution* **9**, 12000-12016 (2019). https://doi.org/https://doi.org/10.1002/ece3.5670
725 46 Prosser, J. I. *et al.* The role of ecological theory in microbial ecology. *Nat Rev Microbiol* **5**, 384-
726 392 (2007). https://doi.org/10.1038/nrmicro1643
727 47 Sterflinger, K. *et al.* Future directions and challenges in biodeterioration research on historic
728 materials and cultural properties. *Int Biodeter Biodegr* **129**, 10-12 (2018).
729 https://doi.org/https://doi.org/10.1016/j.ibiod.2017.12.007
730 48 Wu, Y. *et al.* Monitoring the Deterioration of Masonry Relics at a UNESCO World Heritage Site.
731 *KSCE Journal of Civil Engineering* **25**, 3097-3106 (2021). https://doi.org/10.1007/s12205-021-
732 1716-z

733 49 Zhang, X. W., Ge, Q. Y., Zhu, Z. B., Deng, Y. M. & Gu, J. D. Microbiological community of the
734 Royal Palace in Angkor Thom and Beng Mealea of Cambodia by Illumina sequencing based on
735 16S rRNA gene. *Int Biodeter Biodegr* **134**, 127-135 (2018).
736 https://doi.org/10.1016/j.ibiod.2018.06.018
737 50 Schröer, L., De Kock, T., Cnudde, V. & Boon, N. Differential colonization of microbial
738 communities inhabiting Lede stone in the urban and rural environment. *Sci Total Environ* **733**,
739 139339 (2020). https://doi.org/https://doi.org/10.1016/j.scitotenv.2020.139339
740 51 Qian, Y., Liu, X., Hu, P., Gao, L. & Gu, J.-D. Identifying the major metabolic potentials of
741 microbial-driven carbon, nitrogen and sulfur cycling on stone cultural heritage worldwide. *Sci*
742 *Total Environ* **954**, 176757 (2024).
743 https://doi.org/https://doi.org/10.1016/j.scitotenv.2024.176757
744 52 Grossi, C. E. M. *et al.* Methylobacterium sp. 2A Is a Plant Growth-Promoting Rhizobacteria That
745 Has the Potential to Improve Potato Crop Yield Under Adverse Conditions. *Frontiers in Plant*
746 *Science* **11** (2020). https://doi.org/10.3389/fpls.2020.00071
747 53 Ramond, P., Galand, P. E. & Logares, R. Microbial functional diversity and redundancy: moving
748 forward. *FEMS Microbiology Reviews* **49**, fuae031 (2025).
749 https://doi.org/10.1093/femsre/fuae031
750 54 Tian, L. *et al.* Deciphering functional redundancy in the human microbiome. *Nat Commun* **11**,
751 6217 (2020). https://doi.org/10.1038/s41467-020-19940-1
752 55 Li, H. *et al.* Food provisioning results in functional, but not compositional, convergence of the
753 gut microbiomes of two wild Rhinopithecus species: Evidence of functional redundancy in the
754 gut microbiome. *Sci Total Environ* **858**, 159957 (2023).
755 https://doi.org/https://doi.org/10.1016/j.scitotenv.2022.159957
756 56 Moya, A. & Ferrer, M. Functional Redundancy-Induced Stability of Gut Microbiota Subjected to
757 Disturbance. *Trends Microbiol* **24**, 402-413 (2016). https://doi.org/10.1016/j.tim.2016.02.002
758 57 Tian, L. & Zhang, J. Dynamics of Rabies Epidemics in Vampire Bats. *Complexity* **2020**, 7032451
759 (2020). https://doi.org/https://doi.org/10.1155/2020/7032451
760 58 Talbot, J. M. *et al.* Endemism and functional convergence across the North American soil
761 mycobiome. *PNAS* **111**, 6341-6346 (2014). https://doi.org/10.1073/pnas.1402584111
762 59 Zeng, Q. *et al.* Stable functional structure despite high taxonomic variability across fungal
763 communities in soils of old-growth montane forests. *Microbiome* **11**, 217 (2023).
764 https://doi.org/10.1186/s40168-023-01650-7
765 60 Chen, H. *et al.* Functional Redundancy in Soil Microbial Community Based on Metagenomics
766 Across the Globe. *Front Microbiol* **13** (2022).
767 61 Zhou, J. *et al.* The diversity and ecological significance of microbial traits potentially involved in
768 B12 biosynthesis in the global ocean. *mLife* **2**, 416-427 (2023).
769 https://doi.org/https://doi.org/10.1002/mlf2.12095
770 62 Burke, C., Steinberg, P., Rusch, D., Kjelleberg, S. & Thomas, T. Bacterial community assembly
771 based on functional genes rather than species. *PNAS* **108**, 14288-14293 (2011).
772 https://doi.org/10.1073/pnas.1101591108
773 63 Louca, S. *et al.* Function and functional redundancy in microbial systems. *Nature Ecology &*
774 *Evolution* **2**, 936-943 (2018). https://doi.org/10.1038/s41559-018-0519-1
775 64 Chikina, M., Robinson, J. D. & Clark, N. L. Hundreds of Genes Experienced Convergent Shifts in
776 Selective Pressure in Marine Mammals. *Molecular Biology and Evolution* **33**, 2182-2192 (2016).

https://doi.org/10.1093/molbev/msw112

65 Winemiller, K. O., Fitzgerald, D. B., Bower, L. M. & Pianka, E. R. Functional traits, convergent evolution, and periodic tables of niches. *Ecol Lett* **18**, 737-751 (2015). https://doi.org/https://doi.org/10.1111/ele.12462

66 Nie, Y. *et al.* Species Divergence vs. Functional Convergence Characterizes Crude Oil Microbial Community Assembly. *Front Microbiol* **7** (2016).

67 Li, P. *et al.* Global diversity and biogeography of potential phytopathogenic fungi in a changing world. *Nat Commun* **14**, 6482 (2023). https://doi.org/10.1038/s41467-023-42142-4

68 Gao, C. *et al.* Fungal community assembly in drought-stressed sorghum shows stochasticity, selection, and universal ecological dynamics. *Nat Commun* **11**, 34 (2020). https://doi.org/10.1038/s41467-019-13913-9

69 Wang, B., Zhu, C., Hu, Y., Zhang, B. & Wang, J. Dynamics of microbial community composition during degradation of silks in burial environment. *Sci Total Environ* **883**, 163694 (2023). https://doi.org/https://doi.org/10.1016/j.scitotenv.2023.163694

70 Meng, H., Luo, L., Chan, H. W., Katayama, Y. & Gu, J.-D. Higher diversity and abundance of ammonia-oxidizing archaea than bacteria detected at the Bayon Temple of Angkor Thom in Cambodia. *Int Biodeter Biodegr* **115**, 234-243 (2016). https://doi.org/https://doi.org/10.1016/j.ibiod.2016.08.021

71 Puente-Sánchez, F., Pascual-García, A., Bastolla, U., Pedrós-Alió, C. & Tamames, J. Cross-biome microbial networks reveal functional redundancy and suggest genome reduction through functional complementarity. *Communications Biology* **7**, 1046 (2024). https://doi.org/10.1038/s42003-024-06616-5

72 MacArthur, R. Species packing and competitive equilibrium for many species. *Theoretical Population Biology* **1**, 1-11 (1970). https://doi.org/https://doi.org/10.1016/0040-5809(70)90039-0

73 Advani, M., Bunin, G. & Mehta, P. Statistical physics of community ecology: a cavity solution to MacArthur's consumer resource model. *Journal of Statistical Mechanics: Theory and Experiment* **2018**, 033406 (2018). https://doi.org/10.1088/1742-5468/aab04e

74 Marsland, R., III *et al.* Available energy fluxes drive a transition in the diversity, stability, and functional structure of microbial communities. *PLOS Computational Biology* **15**, e1006793 (2019). https://doi.org/10.1371/journal.pcbi.1006793

75 Sriswasdi, S., Yang, C.-c. & Iwasaki, W. Generalist species drive microbial dispersion and evolution. *Nat Commun* **8**, 1162 (2017). https://doi.org/10.1038/s41467-017-01265-1

76 Wang, B., Qi, M., Ma, Y., Zhang, B. & Hu, Y. Microbiome Diversity and Cellulose Decomposition Processes by Microorganisms on the Ancient Wooden Seawall of Qiantang River of Hangzhou, China. *Microb Ecol* **86**, 2109-2119 (2023). https://doi.org/10.1007/s00248-023-02221-x

77 Wang, B., Zhu, C., Wang, B., Zhang, B. & Hu, Y. Analysis of the biocorrosion community from ancient wooden constructions at Tianluoshan (7000–6300 cal BP), Zhejiang Province, China. *Heritage Science* **12**, 189 (2024). https://doi.org/10.1186/s40494-024-01304-3

78 Zhu, C. *et al.* Application and evaluation of a new blend of biocides for biological control on cultural heritages. *Int Biodeter Biodegr* **178**, 105569 (2023). https://doi.org/https://doi.org/10.1016/j.ibiod.2023.105569

79 Li, J. *et al.* Changes in soil microbial communities at Jinsha earthen site are associated with earthen site deterioration. *BMC Microbiology* **20**, 147 (2020). https://doi.org/10.1186/s12866-

821 020-01836-1
822 80 Wang, X., Wang, B., Hu, Y., Zhang, Z. & Zhang, B. Activity-based protein profiling technology
823 reveals malate dehydrogenase as the target protein of cinnamaldehyde against Aspergillus
824 niger. *Int J Food Microbiol* **417**, 110685 (2024).
825 https://doi.org/https://doi.org/10.1016/j.ijfoodmicro.2024.110685
826 81 Logue, J. B. *et al.* Experimental insights into the importance of aquatic bacterial community
827 composition to the degradation of dissolved organic matter. *ISME J* **10**, 533-545 (2016).
828 https://doi.org/10.1038/ismej.2015.131
829 82 Chen, T. *et al.* The Genome Sequence Archive Family: Toward Explosive Data Growth and
830 Diverse Data Types. *Genomics, Proteomics & Bioinformatics* **19**, 578-583 (2021).
831 https://doi.org/https://doi.org/10.1016/j.gpb.2021.08.001
832 83 Members, C.-N. & Partners. Database Resources of the National Genomics Data Center, China
833 National Center for Bioinformation in 2022. *Nucleic Acids Research* **50**, D27-D38 (2022).
834 https://doi.org/10.1093/nar/gkab951
835 84 Callahan, B. J. *et al.* DADA2: High-resolution sample inference from Illumina amplicon data. *Nat*
836 *Methods* **13**, 581-583 (2016). https://doi.org/10.1038/nmeth.3869
837 85 Bolyen, E. *et al.* Reproducible, interactive, scalable and extensible microbiome data science
838 using QIIME 2. *Nat Biotechnol* **37**, 852-857 (2019). https://doi.org/10.1038/s41587-019-0209-
839 9
840 86 Wang, Q., Garrity, G. M., Tiedje, J. M. & Cole, J. R. Nave Bayesian Classifier for Rapid Assignment
841 of rRNA Sequences into the New Bacterial Taxonomy. *Appl Environ Microbiol* **73**, 5261 (2007).
842 87 Pruesse, E. *et al.* SILVA: a comprehensive online resource for quality checked and aligned
843 ribosomal RNA sequence data compatible with ARB. *Nucleic Acids Res* **35**, 7188-7196 (2007).
844 https://doi.org/10.1093/nar/gkm864
845 88 Nilsson, R. H. *et al.* The UNITE database for molecular identification of fungi: handling dark taxa
846 and parallel taxonomic classifications. *Nucleic Acids Research* **47**, D259-D264 (2019).
847 https://doi.org/10.1093/nar/gky1022
848 89 Fu, L., Niu, B., Zhu, Z., Wu, S. & Li, W. CD-HIT: accelerated for clustering the next-generation
849 sequencing data. *Bioinformatics* **28**, 3150-3152 (2012).
850 https://doi.org/10.1093/bioinformatics/bts565
851 90 Langmead, B. & Salzberg, S. L. Fast gapped-read alignment with Bowtie 2. *Nat Methods* **9**, 357-
852 359 (2012). https://doi.org/10.1038/nmeth.1923
853 91 Buchfink, B., Xie, C. & Huson, D. H. Fast and sensitive protein alignment using DIAMOND. *Nat*
854 *Methods* **12**, 59-60 (2015). https://doi.org/10.1038/nmeth.3176
855 92 Tu, Q., Lin, L., Cheng, L., Deng, Y. & He, Z. NCycDB: a curated integrative database for fast and
856 accurate metagenomic profiling of nitrogen cycling genes. *Bioinformatics* **35**, 1040-1048 (2019).
857 https://doi.org/10.1093/bioinformatics/bty741
858 93 Wickham, H. ggplot2. *WIREs Computational Statistics* **3**, 180-185 (2011).
859 https://doi.org/https://doi.org/10.1002/wics.147
860 94 Dixon, P. VEGAN, a package of R functions for community ecology. *Journal of Vegetation Science*
861 **14**, 927-930 (2003). https://doi.org/https://doi.org/10.1111/j.1654-1103.2003.tb02228.x
862 95 Kembel, S. W. *et al.* Picante: R tools for integrating phylogenies and ecology. *Bioinformatics* **26**,
863 1463-1464 (2010). https://doi.org/10.1093/bioinformatics/btq166
864 96 Nguyen, L.-T., Schmidt, H. A., von Haeseler, A. & Minh, B. Q. IQ-TREE: A Fast and Effective

Stochastic Algorithm for Estimating Maximum-Likelihood Phylogenies. *Molecular Biology and Evolution* **32**, 268-274 (2015). https://doi.org/10.1093/molbev/msu300

97 Zhang, J. M., KP. spaa: An R package for computing species association and niche overlap. . *Research Progress of Biodiversity Conservation in China (in Chinese)* **X**, 165-174 (2014).

98 Pandit, S. N., Kolasa, J. & Cottenie, K. Contrasts between habitat generalists and specialists: an empirical extension to the basic metacommunity framework. *Ecology* **90**, 2253-2262 (2009). https://doi.org/https://doi.org/10.1890/08-0851.1

99 Hao, X. *et al.* Effects on community composition and function Pinus massoniana infected by Bursaphelenchus xylophilus. *BMC Microbiology* **22**, 157 (2022). https://doi.org/10.1186/s12866-022-02569-z

100 Wen, T. *et al.* ggClusterNet: An R package for microbiome network analysis and modularity-based multiple network layouts. *iMeta* **1**, e32 (2022). https://doi.org/https://doi.org/10.1002/imt2.32

101 ggraph: An Implementation of Grammar of Graphics for Graphs and Networks (2025).

102 Csardi, G. & Nepusz, T. The igraph software package for complex network research. *InterJournal, Complex Systems* **1695** (2006).